Transp Porous Med (2017) 119:351–372
DOI 10.1007/s11242-017-0885-1

Exact Solutions for Nonlinear High Retention-Concentration Fines Migration

Y. Yang[1] · **P. Bedrikovetsky**[1]

Received: 28 August 2016 / Accepted: 6 June 2017 / Published online: 29 June 2017

Abstract The paper discusses migration of natural reservoir fines lifted by high-rate or low-salinity water injection. The previous papers used linear analytical model, which is valid for low retention of mobilised fine particles in order to determine the model parameters from breakthrough fines concentration and pressure drop across the core during laboratory core-floods. The current work derives exact analytical solutions for the nonlinear case of high retention-concentration fines migration. The solution exhibits uniform profiles of suspended and retained concentrations ahead of the particle front and steady-state retained concentration behind the front. The obtained type curves allow distinguishing between linear and nonlinear fines migration. The laboratory data exhibit close agreement with the nonlinear model predictions, whereas the linear model poorly matches the laboratory data.

Keywords Fines migration · Colloid · Porous media · Mathematical model · Suspension · Particle capture · Particle detachment · Analytical modelling

List of symbols

Latin

c	Suspended particle concentration (L^{-3})
C	Dimensionless suspended particle concentration
f	Drift-delay factor
k	Permeability (L^2)
L	Core length (L)
p	Pressure ($MT^{-2}L^{-1}$)
s	Accessibility factor

✉ P. Bedrikovetsky
pavel.russia@gmail.com

[1] University of Adelaide, Adelaide, Australia

S	Dimensionless retained particle concentration
S_m	Dimensionless maximum vacancy concentration
t	Time (T)
U	Darcy's velocity (LT^{-1})
U_s	Velocity of particles (LT^{-1})
x	Dimensionless linear coordinate

Greek

α	Constant value of drift-delay factor
β	Formation damage coefficient
λ	Filtration coefficient (L^{-1})
μ	Dynamic viscosity ($ML^{-1}T^{-1}$)
σ	Concentration of retained particles
σ_{cr}	Maximum retention function
σ_m	Maximum vacancy concentration
ϕ	Porosity

Subscripts and Superscripts

f	Front
0	Initial value

1 Introduction

Migration of natural reservoir fines occurs during high-rate or low- salinity flows, which causes high-detaching or low-attaching particle-rock forces (Khilar and Fogler 1998). The resulting mobilisation, migration, and straining of fine particles usually cause significant permeability damage and well productivity decline (Civan 2014; Lagasca and Kovscek 2014). The oil and gas industry employs numerous technologies to fix reservoir fines and prevent permeability decline: injection of water with different salt compositions causing strong fines attachment, nanoparticle injection, combined technologies with the use of rate management, etc. (Habibi et al. 2012; Ahmadi et al. 2013; Arab and Pourafshary 2013). However, so-called fines-assisted low-salinity waterflood can enhance the reservoir sweep: weakening of electrostatic particle-rock attraction under low salinity of injected water yields particle detachment with further migration and size exclusion in thin pores, resulting in permeability decline in the swept zone and slowing water down, i.e. low-salinity waterflooding can act as a mobility control method of enhanced oil recovery (Zeinijahromi et al. 2011). The effects of fines detachment and consequent permeability decline in low-salinity environment can be also used for water production control during aquifer water encroachment into oilfield (Zeinijahromi et al. 2015).

The reliable laboratory-based mathematical modelling of fines migration defines the planning and design of the above technologies. Often, analytical models yield regularisation of ill-posed inverse problems, which is essential for tuning the model parameters from laboratory or field data (Alvarez et al. 2006, 2007). Besides, analytical models provide faster and simpler calculations than the numerical models. The above explains large number of works on analytical modelling of suspension-colloidal flows in porous media (Herzig et al. 1970;

Bedrikovetsky 1993; Sen et al. 2002; Polyanin and Manzhirov 2006; Polyanin and Zaitsev 2011; Yuan et al. 2016; You et al. 2016; Zeinijahromi et al. 2016).

The mathematical model for colloidal-suspension transport in porous media accounts for particle capture by the rock and consequent change of the porous space structure and permeability (Herzig et al. 1970; Bradford et al. 2009; Bradford and Wiegmann 2011; Tufenkji and Elimelech 2004; Elimelech et al. 2013). The following governing system consists of mass balance equations for detached and strained fine particles, straining particles rate, and Darcy's law to account for permeability reduction due to particle straining:

$$\frac{\partial\left(\phi s\left(\sigma\right)c+\sigma\right)}{\partial t}+U\frac{\partial cf\left(\sigma\right)}{\partial x}=0 \tag{1}$$

$$\frac{\partial\sigma}{\partial t}=\lambda\left(\sigma\right)f\left(\sigma\right)Uc \tag{2}$$

$$U=-\frac{k_0}{\mu\left(1+\beta\left(\sigma\right)\sigma\right)}\frac{\partial p}{\partial x}, \tag{3}$$

where ϕ is the porosity, k is the permeability, U is the flow velocity, p is the pressure, σ is the retained particle concentration, c is the suspended particle concentration, λ is the filtration function, s is the accessibility factor, f is the drift-delay factor, μ is the viscosity, and β is the formation damage coefficient. The filtration function λ, accessibility factor s, and drift-delay factor f depend on the retained concentration σ. The fines migrate via the fraction of the porous space $s < 1$ that is accessible to the finite-size particles. The fraction of the overall flux $f(\sigma) < 1$ in Eqs. (1, 2) corresponds to the flux through the accessible pore space only, where the fine particles are transported (Bedrikovetsky 2008). Another interpretation of the fraction $f(\sigma) < 1$ is slow drift of the detached fines along the pore walls (Oliveira et al. 2014; Yang et al. 2016); further in the text we call the function $f(\sigma)$ the drift-delay factor.

The following probabilistic models that are more general than system (1–3) capture stochastic features of suspension-colloidal transport in porous media: random-walk equations (Cortis et al. 2006; Shapiro 2007; Lin et al. 2009; Yuan and Shapiro 2010), trajectory analysis (Payatakes et al. 1973), direct pore scale simulation (Bradford et al. 2009), Boltzmann's kinetics equation (Shapiro and Wesselingh 2008), and population balance models (Sharma and Yortsos 1987; Yuan et al. 2012). In particular, probabilistic upscaling of population balance equations for deep bed filtration with size-distributed pores and mono-size particles yields system (1–3) (Bedrikovetsky 2008).

The initial clean-bed conditions for suspension injection into porous media correspond to the absence of the suspended and retained particles:

$$t=0:c=\sigma=0, \tag{4}$$

whereas the boundary condition corresponds to a given particle concentration c_i in the injected water:

$$x=0:c=c_i. \tag{5}$$

Several mathematical models for fines detachment have been proposed for suspension-colloidal flows (Mays and Hunt 2005, 2007; Tufenkji 2007; Lin et al. 2009; Bradford et al. 2009, 2012, 2013; Elimelech et al. 2013). Kinetics equations for simultaneous fines attachment and detachment contain the relaxation time, yielding the delay in permeability response to rate and salinity alteration. The modified model assumes mechanical equilibrium of particles on the top of the rock or internal cake surface that is subject to the flow in porous space, yielding a maximum attached concentration $\sigma_{cr}(U,\gamma)$ (Bedrikovetsky et al. 2011).

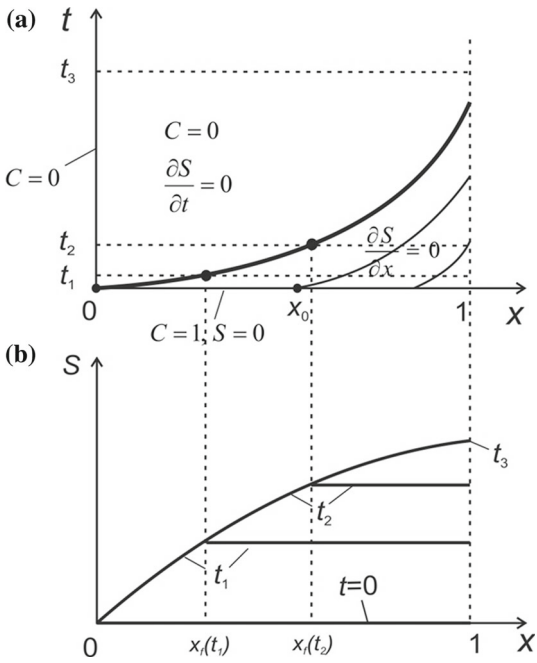

Fig. 1 Exact solution for fines migration: **a** the concentration front and characteristic lines in plane (x, t); **b** retention profiles at three instants and the envelope curve $S(x, t_f(1))$

The particle attachment occurs only until attached concentration reaches its maximum value; the attached concentration remains constant until the mechanical equilibrium is broken. The model exhibits instant detachment of fines, as observed in several laboratory tests (Ochi and Vernoux 1998; Bedrikovetsky et al. 2012). Explicit expressions for maximum attached concentration $\sigma_{cr}(U, \gamma)$ as salinity and rate functions are derived for attached poly-layers of mono-sized fines in cylindrical pores and for attached mono-layers of size-distributed particles (Bedrikovetsky et al. 2011; You et al. 2015). In this work, we assume instant particle detachment.

Therefore, the initial conditions for fines migration under high-rate or low-salinity water injection correspond to instant particle release; the retained particles are considered a part of the porous skeleton (Fig. 1):

$$t = 0 : c = c^0, \sigma = 0, \tag{6}$$

whereas the boundary condition for fines migration corresponds to particle-free water injection:

$$x = 0 : c = 0. \tag{7}$$

The capture of mobilised fines occurs due to attachment or straining. The capture vacancies for attachment are active sites on the rock surface, which are not engaged by the attached fines; the maximum vacancy concentration σ_m corresponds to sites before the attachment (Bradford et al. 2009; Bradford and Wiegmann 2011). For fines straining in thin pore throats, the maximum vacancy concentration is equal to concentration of non-plugged pores (Bradford et al. 2013).

In the case of low fines capture, where the concentration of retained fines is significantly lower than σ_m, the coefficients s, f, λ, and β are constant. System (1, 2) becomes linear. The

exponential quasi steady-state solution of Eqs. (1, 2) subject to initial and boundary conditions (4, 5) for injection of particles in porous media is widely used for analysis of the laboratory data and determination of the filtration coefficient from breakthrough particle concentrations (Tufenkji 2007; Bradford et al. 2009; Elimelech et al. 2013). The linear solution for fine-particle mobilisation during the high-rate injection of particle-free low-salinity water that corresponds to initial and boundary conditions (6, 7) is used for tuning the laboratory data and determining the movable fines concentration (Yang et al. 2016).

In the case of large fines capture, where the concentration of retained fines has the same order of magnitude as σ_m, the filtration coefficient is assumed to be proportional to the available vacancy concentration σ_m-σ (so-called Langmuir blocking filtration function)

$$\lambda(\sigma) = \lambda_0 \left(1 - \frac{\sigma}{\sigma_m}\right). \tag{8}$$

The exact solutions for suspension injection under large-concentration particle retention have been derived for the Langmuir (blocking) filtration function for the case where $s = f = 1$ (Herzig et al. 1970).

The introduction of potential for suspension concentration allows deriving the exact solution of the initial-boundary problem (Polyanin and Manzhirov 2006; Polyanin and Zaitsev 2011) for any arbitrary form of the filtration function $\lambda(\sigma)$. The exact solution of the forward problem allows for regularisation of inverse problems, which determine the filtration and formation damage functions from breakthrough concentration and pressure drop, respectively (Alvarez et al. 2006, 2007). Yet, the exact solutions of governing system (1–3) subject to initial-boundary conditions (6, 7), i.e. the analytical model for nonlinear fines migration at large retention is not in the literature.

In the current work, we derive an exact solution for the fines migration problem for arbitrary filtration, accessibility, and drift-delay functions. The type curves derived from the solution allow for differentiation between the linear and nonlinear suspension-colloidal flows. The exact solution distinguishes the features of fines-migration flows: uniform profiles for suspended and retained concentrations ahead of the concentration front, and no suspended fines at steady state behind the front. The laboratory data exhibit strong agreement with the nonlinear analytical model, while the linear model provides the poor match.

The structure of the text is as follows. Section 2 presents the main assumptions and corresponding dimensionless system for colloidal-suspension flow in porous media. Section 3 derives the exact solution for fines migration for arbitrary forms of functions $s(S)$, $f(S)$, and $\lambda(S)$. Section 4 discusses several particular cases of the exact solution, including Langmuir's blocking function. Section 5 shows the solution-based type curves for suspended and retained concentration and for pressure drop across the core. Section 6 presents the results of solution-based matching of laboratory data. Section 7 discusses our findings. Section 8 concludes the paper.

2 Governing Equations

Consider fine-particle mobilisation, transport, and retaining in porous media due to injection of low-salinity water. The retention rate is proportional to the advective particle flux [see Eq. (2)]. Fine-particle dispersion is negligible compared with the particle advection. Further assumption is that the suspended particles are mono-sized. The advective particle flux is cfU, where f is the drift-delay factor, so the fines velocity is fU/s.

Stabilisation of retained concentration and pressure drop across the core during fines migration occurs after injection of hundreds of pore volumes and is attributed to mobilised fines' rolling and sliding near pore walls at a velocity (fU/s) that is significantly lower than the carrier water velocity (U) (Ochi and Vernoux 1998; Schembre and Kovscek 2005; Schembre et al. 2006; Oliveira et al. 2014). Modelling of suspension-colloidal flows in porous space by Navier–Stokes equations also shows that the particle drift near the rough pore walls has the velocity significantly lower than the injected water velocity (Sefrioui et al. 2013). Several authors mention the two-speed colloidal-suspension flux, where the particle velocity near to matrix surface may be significantly lower than the carrier water velocity (Yuan and Shapiro 2011a, b; Bradford and Wiegmann 2011; Bradford et al. 2012). Model (1–3) describes the case where a rapid mass exchange occurs between fast and slow particle populations across each pore. It results in equal concentrations of particles in the fast and slow fluxes, thus making model (1–3) single-velocity. Model (1–3) and the hypothesis of slow migration of fines in porous media are validated by comparison between the laboratory and modelling data (Yang et al. 2016; Bhattacharya et al. 2016).

The released particle displacement during 1 PVI is negligible compared with the core size L. Therefore, we assume that at the beginning of injection, the mobilised suspended particles already fill the porous space and have not yet been captured by the rock. Instant release of the attached fines followed by changing salinity is assumed also. Those assumptions yield the initial conditions (6), so

$$c^0 = \frac{\sigma_{cr}(\gamma_0) - \sigma_{cr}(\gamma_1)}{\phi} \tag{9}$$

where $\sigma_{cr} = \sigma_{cr}(\gamma)$ is the maximum retention function discussed in Introduction, γ_0 is the initial salinity, and γ_1 is the injected salinity.

The particle capture mechanism is not specified. Usually it is straining of the released particles that contribute to permeability decline during fines migration. Yet, particle attachment, diffusion, or segregation affects the suspended concentration. Below we assume a single retention mechanism; the parameters of changing porous space and capture probability are determined by the retention concentration.

The above assumptions yield the governing equations (1–3).

Introducing dimensionless variables and parameters into system (1–3),

$$x \to \frac{x}{L}, t \to \frac{Ut}{\phi L}, C \to \frac{c}{c^0}, S \to \frac{\sigma}{\phi c^0}, \lambda \to \lambda L, p \to \frac{kp}{\mu L U}, \tag{10}$$

leads to the following dimensionless system:

$$\frac{\partial}{\partial t}[s(S)C + S] + \frac{\partial}{\partial x}[f(S)C] = 0 \tag{11}$$

$$\frac{\partial S}{\partial t} = \lambda(S) f(S) C \tag{12}$$

$$1 = -\frac{1}{1 + \beta\phi c^0 S}\frac{\partial p}{\partial x}. \tag{13}$$

Equation (13) separates from Eqs. (11, 12), i.e. unknowns $C(x, t)$ and $S(x, t)$ are determined from system (11, 12) subject to initial and boundary conditions (6, 7), and then pressure distribution is obtained from Eq. (13).

3 Exact Solution for One-Dimensional Fines Migration

Let us express suspended concentration C from Eq. (12) by introducing potential $\Phi(S)$:

$$C = \frac{\partial \Phi(S)}{\partial t}, \Phi'(S) = \frac{1}{\lambda(S) f(S)}, \Phi(S) = \int_0^S \frac{\mathrm{d}u}{\lambda(u) f(u)}. \tag{14}$$

Substituting expression (14) into Eq. (11) results in

$$\frac{\partial}{\partial t}\left[s(S)\frac{\partial \Phi(S)}{\partial t} + S\right] + \frac{\partial}{\partial x}\left[f(S)\frac{\partial \Phi(S)}{\partial t}\right] = 0. \tag{15}$$

The expression inside the second set of square brackets in Eq. (15) can be represented as a time derivative. This allows changing the order of derivatives over x and t:

$$\frac{\partial}{\partial t}\left[s(S)\frac{\partial \Phi(S)}{\partial t} + S\right] + \frac{\partial}{\partial t}\left[f(S)\frac{\partial \Phi(S)}{\partial x}\right] = 0. \tag{16}$$

Integration of both sides of Eq. (16) in t yields

$$s(S)\frac{\partial \Phi(S)}{\partial t} + S + f(S)\frac{\partial \Phi(S)}{\partial x} = g(x). \tag{17}$$

Initial conditions (6) determine the right side of Eq. (17). At $t = 0$, the first term on the left side of Eq. (17) is

$$t = 0 : s(S)\frac{\partial \Phi(S)}{\partial t} = \frac{s(S)}{\lambda(S) f(S)}\frac{\partial S}{\partial t} = \frac{s(S)}{\lambda(S) f(S)}\lambda(S) f(S) C = s(0). \tag{18}$$

At $t = 0$, the second and third terms on the left side of Eq. (17) equal zero, and Eq. (17) becomes

$$s(S)\frac{\partial \Phi(S)}{\partial t} + S + f(S)\frac{\partial \Phi(S)}{\partial x} = s(0). \tag{19}$$

Substituting the expression for potential $\Phi(S)$ from Eq. (14) into Eq. (19) yields

$$\frac{\partial S}{\partial t} + \frac{f(S)}{s(S)}\frac{\partial S}{\partial x} = \frac{(s(0) - S)\lambda(S) f(S)}{s(S)}. \tag{20}$$

The following system of two ordinary differential equations is a characteristic form of first-order hyperbolic partial differential equation (20) (Logan 2015):

$$\frac{\mathrm{d}x}{\mathrm{d}t} = \frac{f}{s}, \frac{\mathrm{d}S}{\mathrm{d}t} = \frac{(s(0) - S)\lambda(S) f(S)}{s(S)}. \tag{21}$$

The characteristic curve trajectories are shown schematically in Fig. 1.

Let us derive the solution ahead of the concentration front for $x > x_f(t)$. Integrating the second equation in system (21) by separation of variables and accounting for initial conditions (6) yields

$$t = \int_0^S \frac{s(u)\,\mathrm{d}u}{(s(0) - u)\lambda(u) f(u)}. \tag{22}$$

Introducing x as a parameter along the characteristic lines (21) yields

$$\frac{\mathrm{d}t}{\mathrm{d}x} = \frac{s(S)}{f(S)}, \frac{\mathrm{d}S}{\mathrm{d}x} = \lambda(S)(s(0) - S). \tag{23}$$

Integrating the second equation of system (23) by separation of variables and accounting for initial conditions (6) yields

$$x - x_0 = \int_0^S \frac{\mathrm{d}u}{\lambda(u)(s(0) - u)}. \tag{24}$$

Equations (22, 24) define the characteristic curve intercepting point x_0 parametrically (Fig. 1). Either Eq. (22) or (23) determines retained concentration along the characteristic curve.

The concentration front $x = x_\mathrm{f}(t)$ corresponds to $x_0 = 0$ in Eq. (24):

$$x_\mathrm{f}(t) = \int_0^S \frac{\mathrm{d}u}{\lambda(u)(s(0) - u)}. \tag{25}$$

Thus, Eqs. (22, 25) determine the concentration front trajectory via the parameter S.

The arrival time $t_\mathrm{f}(x)$ is given by Eqs. (22, 24) for $x_0 = 0$:

$$t_\mathrm{f}(x) = \int_0^S \frac{s(u)\,\mathrm{d}u}{(s(0) - u)\lambda(u) f(u)}, x = \int_0^S \frac{\mathrm{d}u}{\lambda(u)(s(0) - u)}. \tag{26}$$

Suspension concentration $C(x, t)$ is determined from the first expression of Eq. (14) for a known solution $S(x, t)$.

Exact solution (22) is determined for the domain $x > x_\mathrm{f}(t)$ in the plane (x, t) (Fig. 1). Equation (22) shows that retention concentration ahead of the front is independent of x and depends only on time t.

Now let us derive the solution behind the concentration front for $x < x_\mathrm{f}(t)$.

Substituting Eq. (12) into the left side of Eq. (11) and differentiating yields

$$\frac{\partial C}{\partial t} + \frac{f(S)}{s(S)}\frac{\partial C}{\partial x} = -C\left[\frac{\lambda(S) f(S)}{s(S)} + \frac{f'(S)}{s(S)}\frac{\partial S}{\partial x}\right] - C^2\frac{s'(S)\lambda(S) f(S)}{s(S)}. \tag{27}$$

The characteristic form of Eq. (27) is:

$$\frac{\mathrm{d}x}{\mathrm{d}t} = \frac{f(S)}{s(S)}, \frac{\mathrm{d}C}{\mathrm{d}t} = -C\left[\frac{\lambda(S) f(S)}{s(S)} + \frac{f'(S)}{s(S)}\frac{\partial S}{\partial x}\right] - C^2\frac{s'(S)\lambda(S) f(S)}{s(S)}. \tag{28}$$

Ordinary differential equation (28) with initial-boundary condition (6) shows that $C(x, t) = 0$ for $x < x_\mathrm{f}(t)$. Therefore, it follows from Eq. (12) that $\mathrm{d}S/\mathrm{d}t = 0$ behind the concentration front, i.e. retained concentration is steady state behind the concentration front:

$$x < x_\mathrm{f}(t) : C = 0, S(x, t) = S(x, t_\mathrm{f}(x)). \tag{29}$$

At the instant of system stabilisation, the concentration front reaches the outlet. No retention or suspension flow occurs in the core afterwards. The stabilisation instant $t_\mathrm{f}(1)$ is determined from Eq. (26) for $x = 1$. The stabilised retention profile $S(x, t_\mathrm{f}(1))$ for $t > t_\mathrm{f}(1)$ is also determined from Eqs. (26, 29) for $x = 1$.

Finally, Eq. (22) determines retained concentration $S(x, t)$ ahead of the concentration front, yielding a uniform profile. Equations (26, 29) determine retained concentration $S(x, t)$ behind the front, yielding a steady-state distribution. Suspension concentration ahead of the front is determined from Eq. (14) for known retained concentration ahead of the front. Suspension concentration is zero behind the front.

Expressing pressure gradient from Eq. (13), we calculate pressure drop across the core:

$$\Delta p = -\int_0^1 \frac{\partial p}{\partial x}\mathrm{d}x = \int_0^1 \left(1 + \beta\phi c^0 S\left(x,t\right)\right)\mathrm{d}x = 1 + \beta\phi c^0 \int_0^1 S\left(x,t\right)\mathrm{d}x. \tag{30}$$

4 Simplified Cases of the Analytical Model

Constant accessibility and drift delay: $s(S) = const$, $f(S) = const$. Characteristic speed in Eq. (21) becomes constant. The front trajectory (26) becomes a straight line

$$x_{\mathrm{f}} = \frac{f}{s}t. \tag{31}$$

Equation (22) with constant s and f defines $S(t)$ and $C(t)$ ahead of the concentration front. Equations (22, 29) for steady-state retention distribution behind the front become

$$x = \int_0^S \frac{\mathrm{d}u}{\left(s-u\right)\lambda\left(u\right)}. \tag{32}$$

Equation (32) shows that retention distribution is x-dependent only and is independent of the drift-delay factor.

Langmuir blocking filtration function and constant accessibility and drift delay. For filtration function (8)

$$\lambda\left(S\right) = \lambda_0\left(1 - bS\right), b = S_m^{-1}, \tag{33}$$

the integral (22) becomes

$$\frac{f}{s}t = \int_0^S \frac{\mathrm{d}u}{\left(s\left(0\right)-u\right)\lambda_0\left(1-\frac{S}{S_m}\right)}. \tag{34}$$

It allows for the explicit formula for retention distribution ahead of the front:

$$S(x,t) = \frac{\lambda_0 s\left(\mathrm{e}^{\left(\lambda_0 - \frac{\lambda_0}{S_m}s\right)\frac{f}{s}t} - 1\right)}{\lambda_0 \mathrm{e}^{\left(\lambda_0 - \frac{\lambda_0}{S_m}s\right)\frac{f}{s}t} - \frac{\lambda_0}{S_m}s}. \tag{35}$$

The suspension concentration follows from Eq. (14):

$$C(x,t) = \frac{\left(\lambda_0 - \frac{\lambda_0}{S_m}s\right)}{\lambda_0 \mathrm{e}^{\left(\lambda_0 - \frac{\lambda_0}{S_m}s\right)\frac{f}{s}t} - \frac{\lambda_0}{S_m}s}. \tag{36}$$

The retention distribution behind the front follows from Eq. (32):

$$S(x,t) = \frac{\lambda_0 s\left(\mathrm{e}^{\left(\lambda_0 - \frac{\lambda_0}{S_m}s\right)x} - 1\right)}{\lambda_0 \mathrm{e}^{\left(\lambda_0 - \frac{\lambda_0}{S_m}s\right)x} - \frac{\lambda_0}{S_m}s}. \tag{37}$$

Constant accessibility, drift delay, and filtration coefficient. Assuming s, f, and λ constant, and infinite S_m, from Eqs. (35, 36), we obtain the solution

$$S(x,t) = \begin{cases} s\left(1 - e^{-\frac{f}{s}\lambda_0 t}\right), & x \geq \frac{f}{s}t \\ s\left(1 - e^{-\lambda_0 x}\right), & x < \frac{f}{s}t \end{cases}, \tag{38}$$

$$C(x,t) = \begin{cases} e^{-\lambda_0 \frac{f}{s}t}, & x \geq \frac{f}{s}t \\ 0, & x < \frac{f}{s}t \end{cases}. \tag{39}$$

Linear functions for filtration, accessibility, and drift delay. Integrals in Eqs. (22) and (26) contain polynomials of third and second orders and can be solved explicitly.

5 Type Curves for Concentrations and Pressure Drop

In this section, for the case where the particles are significantly smaller than pores, i.e. $s = 1$, we calculate the type curves for retention and suspension concentrations and for the pressure drop across the core. Fines roll and slide along pore walls; thus, $f(S)/s(S) = \alpha \ll 1$. Particle capture is governed by the Langmuir blocking function, Eq. (33). The calculation results are presented in Figs. 2, 3, and 4.

The case $b = 0$ ($S_m = \infty$) corresponds to constant filtration coefficient. The solution is given by formulae (38, 39), showing that the logarithm of breakthrough concentration is linear versus time. Thus, the breakthrough concentration in semilogarithmic coordinates is given by a straight line (Fig. 2). Its tangent is equal to $\alpha\lambda_0$. The straight line crosses the vertical axes at ordinate lnc^0. The dimensional breakthrough concentration decreases from the initial value c^0. Using two breakthrough concentration measurements and plotting the corresponding straight line in semilogarithmic coordinates allows for calculation of the initial suspended concentration c^0, which avoids the errors in concentration measurement at the beginning of injection.

Langmuir's cases with $S_m > 0$, in which filtration coefficient decreases during filling the retention vacancies from $S = 0$ to $S = S_m$, correspond to convex retention curves (curves 1 and 2 in Fig. 3a) and concave breakthrough curves (curves 1 and 2 in Fig. 3b). The cases where the filtration function increases during the retention ($b < 0$) correspond to concave retention curves (curves 4 and 5 in Fig. 3a) and convex breakthrough curves (curves 4 and 5 in Fig. 3b).

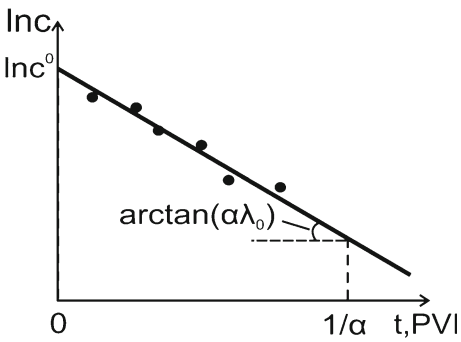

Fig. 2 Breakthrough concentration in semilogarithmic coordinates for low-retention fines migration

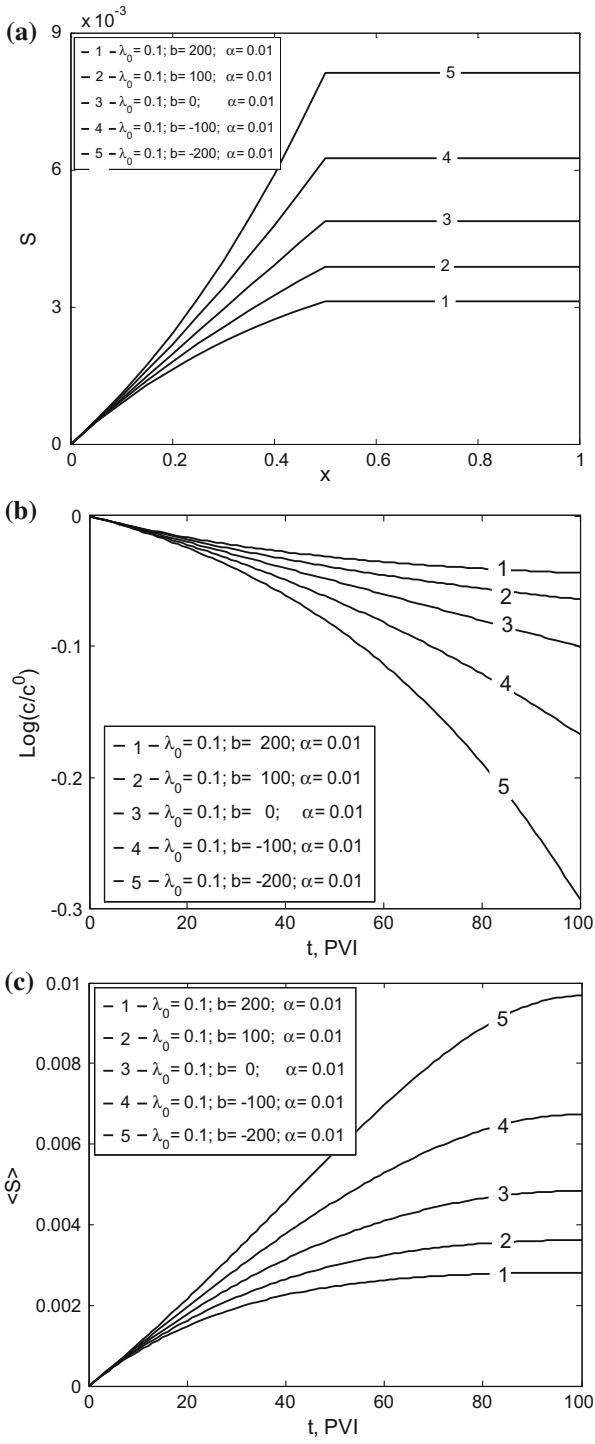

Fig. 3 Effects of maximum vacancy concentration $S_m = 1/b$ on fines migration: **a** retention profiles after 50 PVI; **b** breakthrough concentration; **c** average retention concentration versus time

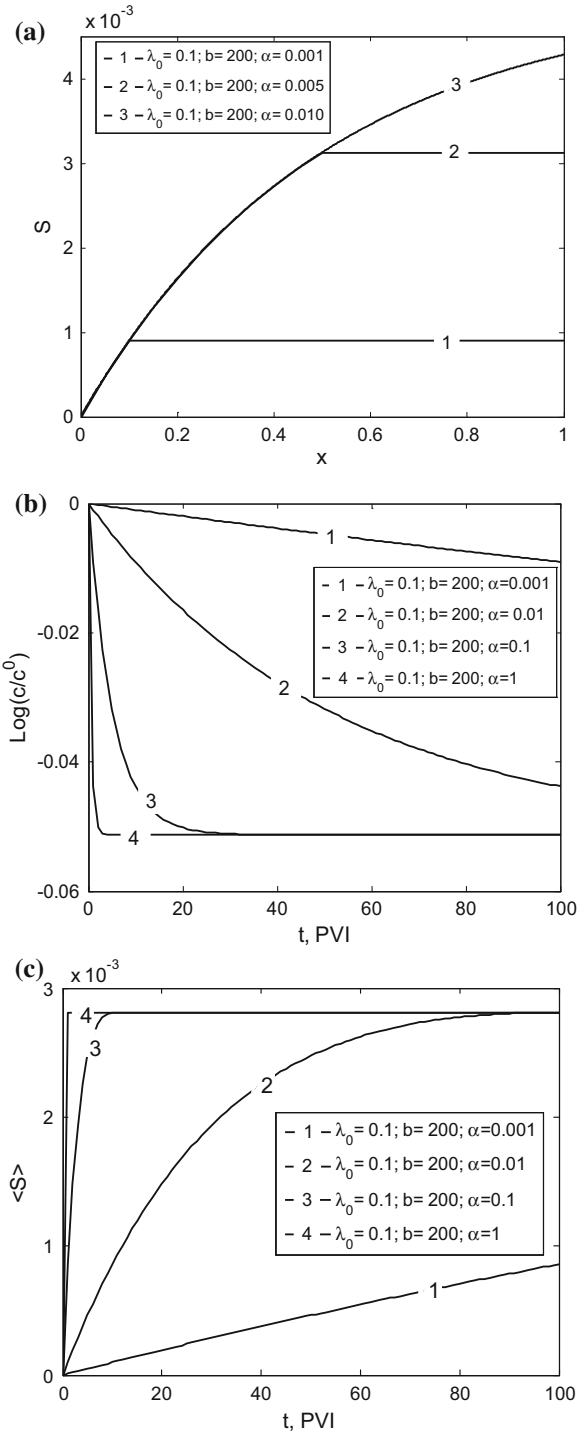

Fig. 4 Effects of drift-delay factor α on fines migration: **a** retention profiles after 100 PVI; **b** breakthrough concentration; **c** average retention concentration versus time

Figures 3a and 4a show the retention profiles. It follows from Eqs. (22, 29) that retention profile is uniform ahead of the concentration front and steady state behind the front. So, at each point x_0 of the reservoir before the front arrival, $S(x_0, t)$ grows monotonically from zero to the maximum, $S(x_0, t_f(x_0))$, at the moment of the front arrival. $S(x_0, t)$ then remains constant. Therefore, there exists an envelope profile $S(x, t_f(1))$. From the instant of the breakthrough $t > t_f(1)$, the retention profile coincides with the envelope curve. The retention profiles in Fig. 3a correspond to $t = 50$ PVI, which is before the front arrival at the core outlet. Cases 1 and 2 in Fig. 4a also show the retention concentration before the front arrival; however, the front already arrived in case 3.

The lower the maximum vacancy concentration S_m, the higher the constant b, the lower the filtration function, the lower the retention profile, and the higher the breakthrough concentration (Fig. 3a, b).

According to formula (30), the pressure drop across the column is linearly dependent on the average retention concentration $<S>$. Figure 3c shows that the higher the maximum vacancy concentration S_m, the larger the averaged concentration and the higher the pressure drop.

Figure 4 shows the effect of drift-delay factor $f = \alpha$ ($s = 1$) on retained and breakthrough concentrations and on the average retention concentration. The higher the f, the faster the fine particles move and arrive (Fig. 4a), the larger the particle flux and retention concentration (Fig. 4a), and the lower the suspended concentration (Fig. 4b).

Monotonic growth of the average retention concentration is shown in Fig. 4c. At the instant $1/\alpha$, the pressure drop stabilises. The higher the drift-delay factor $f = \alpha$, the sooner that stabilisation occurs.

6 Matching the Experimental Data

In this section, the analytical model (35–37) matches the laboratory data from 12 experiments. The nonlinear least square method (improved Levenberg–Marquardt procedure) was applied for matching the data (More 1977; Coleman and Li 1996). The optimisation algorithm implemented in MATLAB was used (MatLab 2013). The Levenberg–Marquardt method acts more like a gradient descent method when the parameters are far from their optimal value, and acts more like the Gauss–Newton method when the parameters are close to their optimal value.

Grolimund et al. (2001) injected water into a column filled by non-calcareous soil material that consisted of 16% sand, 18% clay, and 66% loam. In each experiment, particle release was initiated by reduction of injected water salinity if compared with the formation of water salinity. The ionic strengths of the injected water are shown in second column of Table 1. Sodium was used as a main cation in all experiments. Figure 5 shows the breakthrough concentration of mobilised fines for ionic strength reduction from 500 to 20 mM. The effects of salt concentrations on particle mobilisation were investigated in several chemical environments. Figures 6, 7, 8, and 9 show the effect of injected salinity on fines production in the presence of chloride, malonate, phthalate, and azide, respectively.

The nonlinear model (Eqs. 35–37) and linear model (Eqs. 38, 39) match the breakthrough curve by the error minimisation. For all tests, the laboratory data show close agreement with the nonlinear model, whereas the results of the linear model significantly deviate from the experimental breakthrough curves. Table 2 presents the obtained values of the tuning parameters α, λ_0, and S_m for the nonlinear model in columns 3, 4, and 5, respectively. The

Table 1 Tuning parameters for fines-migration tests in the presence of various anions and salt concentrations

Anion	$[N_a^+]$ (mM)	Nonlinear model				Linear model
		α	λ_0	S_m	$S(1, t_f(1))/S_m$	$\alpha\lambda_0$
No additional anions	20	9.25E−3	27.7	0.024	0.98	4.22E−3
Chloride	10	1.99E−3	27.87	3.90E−4	0.98	8.67E−3
	20	1.23E−3	15.87	2.44E−5	0.94	4.28E−3
	40	1.08E−3	6.266	1.09E−6	0.78	3.21E−3
Malonate	20	1.10E−3	119.7	4.42E−3	0.99	5.25E−3
	40	1.61E−3	65.08	1.55E−3	0.99	7.11E−3
	80	3.93E−3	22.35	2.32E−4	0.99	1.30E−2
Phthalate	20	4.11E−3	4.951	4.09E−6	0.89	3.70E−3
	40	4.22E−3	5.445	7.90E−7	0.97	6.27E−3
Azide	20	2.72E−3	8.785	2.34E−6	0.93	5.18E−3
	40	2.72E−3	8.785	2.34E−6	0.93	5.18E−3

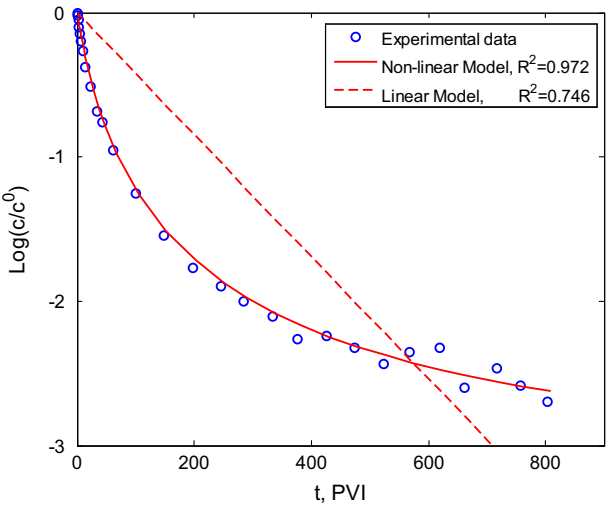

Fig. 5 Matching the laboratory data from mobilisation experiment of colloidal particles in natural porous material

obtained parameters vary in the common intervals typical for suspension-colloidal flows in natural rocks (Al-Abduwani 2005; Al-Abduwani et al. 2005; Alvarez et al. 2006, 2007; Civan 2014; Oliveira et al. 2014).

The sixth column of Table 1 shows the ratio between maximum retained concentration $S(1, t_f(1))$ reached in test at the outlet and the corresponding maximum vacancy concentration S_m. The ratios vary between 0.78 and 0.99, showing that the retention concentration is not negligible compared with S_m, i.e. the linear model (37, 38) is not valid for the test conditions. It explains the high agreement between the laboratory and nonlinear modelling data, and the poor fit by the linear model.

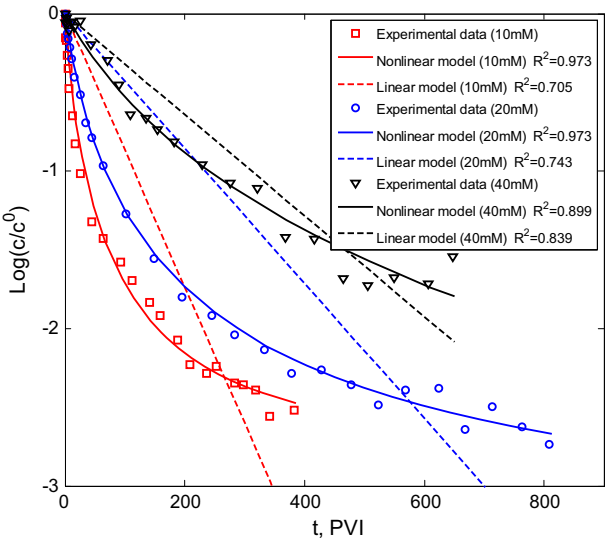

Fig. 6 Dependence of the mobilisation of colloidal particles from a natural rock in the presence of chloride, on salt concentration: 10 mM (*squares*), 20 mM (*circles*), and 40 mM (*triangles*)

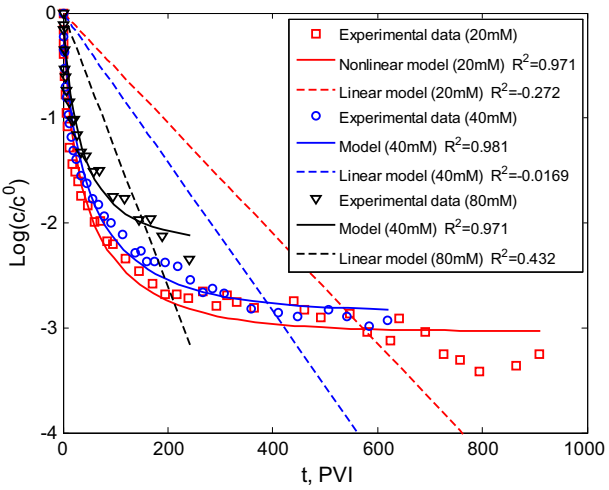

Fig. 7 Dependence of the mobilisation of colloidal particles from a natural porous material in the presence of malonate, on salt concentration: 20 mM (*squares*), 40 mM (*circles*), and 80 mM (*triangles*)

Solution (35) shows that maximum retention concentration $S(1, t_f(1))$ is less than the maximum vacancy concentration S_m and tends to S_m for semi-infinite core. The values of mobilised particle speeds $\alpha = f/s$ in Table 1 are very low, i.e. full system stabilisation occurs after 110–1000 PVI (which is $1/\alpha$). The injection periods in the tests have the same order of magnitude. This explains the values of the ratio $S(1, t_f(1))/S_m$ that are close to one.

Bhattacharya et al. (2016) injected fresh Milli-Q water into an artificial core packed by 90% sand and 10% kaolinite and initially saturated by water with salinity 10 mM. The breakthrough concentration and pressure drop across the core, measured during this injection

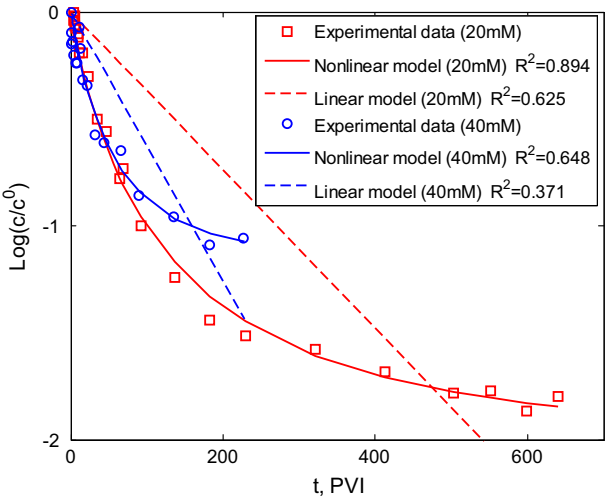

Fig. 8 Dependence of the mobilisation of colloidal particles from a natural rock in the presence of phthalate, on salt concentration: 20 mM (*squares*), 40 mM (*circles*)

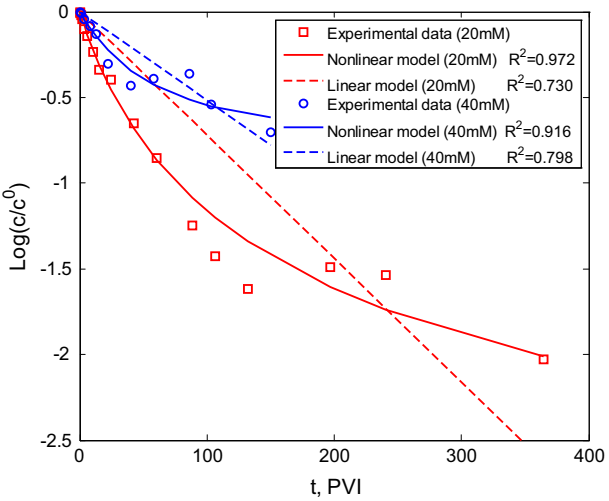

Fig. 9 Dependence of the mobilisation of colloidal particles from a natural porous material in the presence of azide, on salt concentration: 20 mM (*squares*), 40 mM (*circles*)

Table 2 Tuning parameters from breakthrough fines concentration and pressure drop for kaolinite fines migration

Model	α	λ_0	S_m	c^0	$\beta\, c^0$	$S(1, t_f(1))/S_m$
Nonlinear model	0.010	17.16	0.638	7.750e−6	1.434	0.99
Linear model	0.012	1.548	∞	7.750e−6	2.656	–

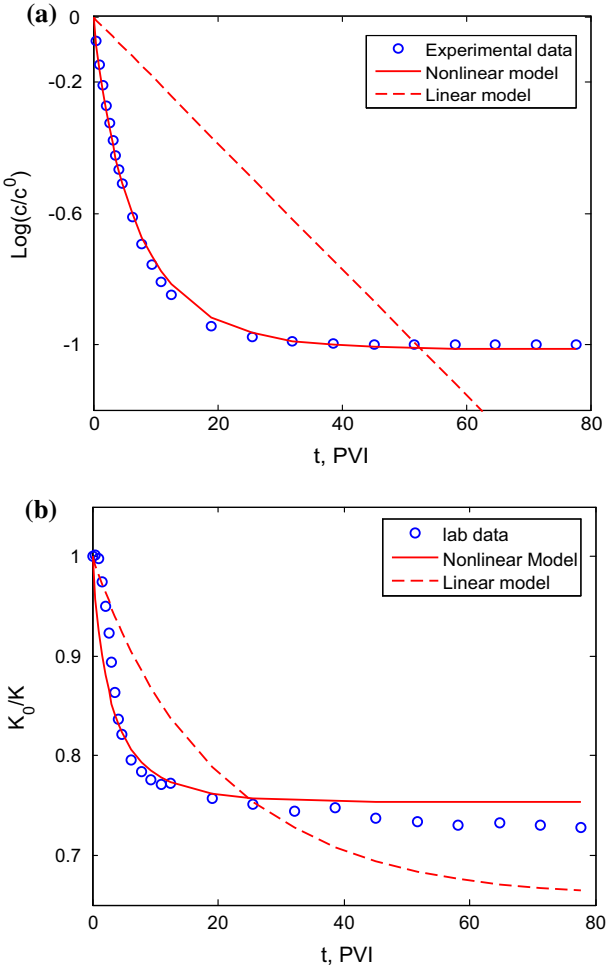

Fig. 10 Matching the fines breakthrough and pressure drop data on fines migration in natural reservoir core: **a** breakthrough concentration; **b** average permeability across the core. The coefficient of determination is $R^2 = 0.879$ for the linear model and $R^2 = 0.998$ for the nonlinear model

test, are presented in Fig. 10. The figure shows high agreement in breakthrough concentration and permeability between the experiment and the nonlinear model, but significant deviation from the linear model. The ratio $S(1, t_f(1))/S_m$ was equal to 0.99, which explains the poor match of the data by the linear model.

7 Discussion

The exact analytical solution for fines migration is given by the set of formulae (22, 26, 29) for any arbitrary functions $s(\sigma)$, $f(\sigma)$, and $\lambda(\sigma)$. Equation (22) determines retention concentration ahead of the front, where the retention concentration is independent of x and depends on time t only. This property is the consequence of the uniform initial distribution of

suspension concentration. The conditions for deep bed filtration are the same for all particles that are situated at any point x at $t = 0$, thus $S = S(t)$ and $C = C(t)$ ahead of the front. The front trajectory is given parametrically by Eq. (26). Suspended concentration equals zero behind the front, due to particle-free water injection. Retained concentration at any point x reaches its maximum and stabilises at the instant when the front passes point x, as given by Eq. (29).

For constant accessibility and drift-delay functions, the concentration front moves with constant speed f/s, and the retention profile behind the front is independent of the drift-delay factor.

For high retention concentration, the laboratory data closely agreed with the nonlinear Langmuir model but not with the linear model. At low retention concentration, where maximum value of the retention concentration is significantly smaller than the maximum vacancy concentration, the results of linear and nonlinear modelling agree highly with the laboratory data.

The close match of the breakthrough concentration and pressure drop does not validate the fines-migration model (1–3). Simultaneous model matching of breakthrough concentration and pressure drop histories, and the retention profile, where the number of model constants is lower than the number of degrees of freedom of the laboratory dataset, would allow the model's validity to be tested. The above data are available for suspension-colloidal injection (Mays and Hunt 2005, 2007); the corresponding model validation has been performed by Al-Abduwani (2005) and Al-Abduwani et al. (2005). To our knowledge, there are no published laboratory data on breakthrough concentration and pressure drop histories, and the retention profile for fines migration.

The laboratory data on breakthrough concentration and pressure drop across the column agree closely with the analytical model based on Langmuir's blocking filtration function (Fig. 10). Yet, the quality of the match can be improved by using a two-parametric equation for permeability reduction. The mono-parametric permeability reduction model given by Eq. (3) follows from ignoring the second- and higher-order terms in Taylor's series for the function $k(0)/k(\sigma)$. Keeping the second-order term yields the second-order polynomial in the denominator in Eq. (3), which was used by Al-Abduwani (2005). The second formation damage coefficient could also be introduced by using the power $(1 + \beta\sigma)^n$, $n \neq 1$ in the denominator of Eq. (3) (Bailey et al. 2000).

The model assumes instant particle release. It corresponds to either negligible relaxation time in the kinetic model with simultaneous attachment and detachment (Tufenkji 2007; Bradford and Wiegmann 2011; Bradford et al. 2012) or the maximum attached-concentration model (Bedrikovetsky et al. 2011).

The exact solutions derived can be used for planning and design of laboratory tests on fines migration—reliable prediction of breakthrough and suspended concentrations and pressure drop allows determining the sample timing, sample volumes, and injection rates where those are feasible, defining which pressure transducers should be used, etc. The type curves and the features of the concentration distributions allow interpretation of the laboratory data. The exact solutions permit the determination of the filtration function and the accessibility and drift-delay factors from the coreflood data.

The derived exact solutions for one-dimensional flow can be used in stream-line simulators for quasi-3D simulation in natural reservoirs. The exact solutions can be also used for upscaling of filtration, accessibility, and drift-delay coefficients in the heterogeneous flow patterns using the stream-line modelling.

The assumptions of the model formulated in Sect. 2 correspond to corefloods with constant initial and injected salinities and slow migration of mobilised fines. More general equations

that can be extended for 3D two-phase flows in oilfields, capture continuous fines release during arrival of the salinity wave and kinetics of particle attachment, where the attached concentration is below the maximum retention concentration. Mass balance equation accounts for attached, suspended and retained particles:

$$\frac{\partial\left(\phi s\left(\sigma\right)c+\sigma_a+\sigma\right)}{\partial t}+U\frac{\partial cf\left(\sigma\right)}{\partial x}=0 \tag{40}$$

If the attached concentration is below the maximum retention value, the attachment occurs, and the rate is given by the linear kinetics equation:

$$\begin{aligned}\frac{\partial\sigma_a}{\partial t}&=\lambda_a f\left(\sigma\right)Uc,\sigma_a<\sigma_{cr}\left(\gamma\right)\\ \sigma_a&=\sigma_{cr}\left(\gamma\right)\end{aligned} \tag{41}$$

Here σ_a and λ_a correspond to particle attachment, which stops when the attached concentration reaches its maximum value $\sigma_{cr}=\sigma_{cr}(\gamma)$.

The continuity equation for salt includes its advective and dispersive fluxes:

$$\frac{\partial\left(\phi\gamma\right)}{\partial t}+U\frac{\partial\gamma}{\partial x}=D\frac{\partial^2\gamma}{\partial x^2} \tag{42}$$

The kinetics of different mechanisms of particle capture than attachment is given by Eq. (2). Equation (3) captures the formation damage and flux alteration due to the particle capture.

The initial and boundary conditions are:

$$\begin{aligned}&t=0:c=0,\gamma=\gamma_0,\sigma=0,\sigma_a=\sigma_{a0},\\ &x=0:c=0,\gamma=\gamma_1\end{aligned} \tag{43}$$

System of five equations (2, 3, 40–42) subject to initial and boundary conditions (43) determines the following unknowns: $\sigma(x,t)$, $c(x,t)$, $\sigma_a(x,t)$, $\gamma(x,t)$ and $p(x,t)$.

For the case where

$$\sigma_{a0}=\sigma_{cr}\left(\gamma_0\right),\gamma_1<\gamma_0,D=0,t\gg1,$$

the above-formulated problem (2, 3, 40–43) degenerates into the problem (1–3, 6, 7) solved in the present work.

8 Conclusions

Exact integration of nonlinear equations for fines migration in porous media and matching the experimental data allows drawing the following conclusions.

The problem of slow fines migration with varying filtration function that accounts for varying accessibility and drift-delay factors allows for exact solution. Distributions of suspended and retained concentrations along with the concentration front trajectory are expressed by implicit formulae.

The solution shows that suspended and retained concentrations ahead of the concentration front depend on time only, i.e. their profiles are uniform. Suspended concentration behind the front equals zero, and the retention concentration is steady state.

If accessibility and drift-delay factors are constant, the concentration front propagates with constant velocity and the retained concentration behind the front is independent of the drift-delay factor.

For the case of Langmuir blocking function and constant accessibility and drift-delay factors, suspended and retained concentrations are expressed by an explicit analytical nonlinear model, which exhibits high agreement with experimental data.

The typical properties of the suspended and retained concentrations are as follows: existence of the envelope curve for retention profiles that determines uniform distribution ahead of the front and steady-state distribution behind the front; concave breakthrough curves for increasing filtration function and convex breakthrough curves for decreasing filtration function in semilogarithmic coordinates; and straight-line breakthrough curve during short after-breakthrough period for low-varying filtration coefficient, allowing determining model constants c^0 and $\alpha\lambda_0$.

Acknowledgements The authors are grateful to Prof Y Osipov (Moscow State University of Civil Engineering) and Dr Z You (the University of Adelaide) for discussion of the analytical model, and to Dr A Badalyan (the University of Adelaide) for providing the laboratory data. Many thanks are due to David H. Levin (Murphy, NC, USA) who provided professional English-language editing of this article.

References

Ahmadi, M., Habibi, A., Pourafshary, P., Ayatollahi, S.: Zeta-potential investigation and experimental study of nanoparticles deposited on rock surface to reduce fines migration. J. Soc. Pet. Eng. SPEJ **18**(03), 534–544 (2013)

Al-Abduwani, F.: Internal filtration and external filter cake build-up in sandstones. Ph.D. thesis, Delft University of Technology, Delft, The Netherlands (2005)

Al-Abduwani, F., Shirzadi, A., Broek, W.M., Currie, P.: Formation damage vs. solid particles deposition profile during laboratory-simulated produced-water reinjection. J. Soc. Pet. Eng. SPEJ **10**(02), 138–151 (2005)

Alvarez, A.C., Bedrikovetsky, P.G., Hime, G., Marchesin, A.O., Marchesin, D., Rodrigues, J.R.: A fast inverse solver for the filtration function for flow of water with particles in porous media. Inverse Probl. **22**(1), 69–88 (2006)

Alvarez, A.C., Hime, G., Marchesin, D., Bedrikovetsky, P.G.: The inverse problem of determining the filtration function and permeability reduction in flow of water with particles in porous media. J. Transp. Porous Media **70**(1), 43–62 (2007)

Arab, D., Pourafshary, P.: Nanoparticles-assisted surface charge modification of the porous medium to treat colloidal particles migration induced by low salinity water flooding. Colloids Surf. A Physicochem. Eng. Asp. **436**, 803–814 (2013)

Bailey, L., Boek, E.S., Jacques, S.D.M., Boassen, T., Selle, O.M., Argillier, J.F., Longeron, D.G.: Particulate invasion from drilling fluid. J. Soc. Pet. Eng. SPEJ **5**(4), 412–419 (2000)

Bedrikovetsky, P.: Mathematical Theory of Oil and Gas Recovery. Kluwer Academic Publishers, Dordrecht (1993)

Bedrikovetsky, P.: Upscaling of stochastic micro model for suspension transport in porous media. J. Transp. Porous Media **75**(3), 335–369 (2008)

Bedrikovetsky, P., Siqueira, F.D., Furtado, C.A., Souza, A.L.S.: Modified particle detachment model for colloidal transport in porous media. Transp. Porous Media **86**(2), 353–383 (2011)

Bedrikovetsky, P., Zeinijahromi, A., Siqueira, F.D., Furtado, C., de Souza, A.L.S.: Particle detachment under velocity alternation during suspension transport in porous media. Transp. Porous Media **91**(1), 173–197 (2012)

Bhattacharya, S.S., Paitaridis, J., Pedler, A., Badalyan, A., Yang, Y., Carageorgos, T., Bedrikovetsky, P., Warren, D., Lemon, N.: Fines mobilisation by low-salinity water injection: 3-point-pressure tests. SPE paper 178974 presented at the International Conference and Exhibition on Formation Damage Control held in Lafayette, LA, USA (2016)

Bradford, S.A., Wiegmann, P.: Pore-scale simulations to determine the applied hydrodynamic torque and colloidal mobilisation. Vadose Zone J. **10**, 252–261 (2011)

Bradford, S.A., Kim, H.N., Haznedaroglu, B.Z., Torkzaban, S., Walker, S.L.: Coupled factors influencing concentration-dependent colloid transport and retention in saturated porous media. J. Environ. Sci. Technol. **43**(18), 6996–7002 (2009)

Bradford, S.A., Kim, H., Simunek, J.: Modeling colloid and microorganism transport and release with transients in solution ionic strength. Water Resour. Res. **48**, W09509 (2012)

Bradford, S.A., Torkzaban, S., Shapiro, A.A.: A theoretical analysis of colloid attachment and straining in chemically heterogeneous porous media. Langmuir **29**(23), 6944–6952 (2013)
Civan, F.: Reservoir Formation Damage, 3rd edn. Gulf Professional Publishing, Burlington (2014)
Coleman, T.F., Li, Y.: An interior, trust region approach for nonlinear minimization subject to bounds. SIAM J. Optim. **6**(2), 418–445 (1996)
Cortis, A., Harter, T., Hou, L., Atwill, E.R., Packman, A.I., Green, P.G.: Transport of *Cryptosporidium parvum* in porous media: long-term elution experiments and continuous time random walk filtration modeling. Water Resour. Res. **42**(12), W12S13 (2006). doi:10.1029/2006WR004897
Elimelech, M., Gregory, J., Jia, X.: Particle Deposition and Aggregation: Measurement, Modelling and Simulation. Butterworth-Heinemann, Oxford (2013)
Grolimund, D., Barmettler, K., Borkovec, M.: Release and transport of colloidal particles in natural porous media: 2. Experimental results and effects of ligands. Water Resour. Res. **37**(3), 571–582 (2001)
Habibi, A., Ahmadi, M., Pourafshary, P., Al-Wahaibi, Y.: Reduction of fines migration by nanofluids injection: an experimental study. J. Soc. Pet. Eng. SPEJ **18**(02), 309–318 (2012)
Herzig, J.P., Leclerc, D.M., Goff, P.L.: Flow of suspensions through porous media-application to deep filtration. Ind. Eng. Chem. Res. **62**(5), 8–35 (1970)
Khilar, K.C., Fogler, S.: Migration of Fines in Porous Media. Kluwer Academic Publishers, Dordrecht (1998)
Lagasca, J.R.P., Kovscek, A.R.: Fines migration and compaction in diatomaceous rocks. J. Pet. Sci. Eng. **122**, 108–118 (2014)
Lin, H.-K., Prydko, L.P., Walker, S., Zandi, R.: Attachment and detachment rate distributions in deep-bed filtration. Phys. Rev. E **79**(4), 046321 (2009)
Logan, D.: Applied Partial Differential Equations, 3rd edn. Springer, New York (2015)
MatLab MathWorks, Inc, Natick, Massachusetts (2013)
Mays, D.C., Hunt, J.R.: Hydrodynamic aspects of particle clogging in porous media. J. Environ. Sci. Technol. **39**(2), 577–584 (2005)
Mays, D.C., Hunt, J.R.: Hydrodynamic and chemical factors in clogging by montmorillonite in porous media. J. Environ. Sci. Technol. **41**(16), 5666–5671 (2007)
More, J.J.: The Levenberg–Marquardt algorithm: implementation and theory. In: Watson, G.A. (ed.) Numerical Analysis. Lecture Notes in Mathematics 630, pp. 105–116. Springer, Berlin (1977)
Ochi, J., Vernoux, J.F.: Permeability decrease in sandstone reservoirs by fluid injection: hydrodynamic and chemical effects. J. Hydrol. **208**(3), 237–248 (1998)
Oliveira, M., Vaz, A., Siqueira, F., Yang, Y., You, Z., Bedrikovetsky, P.: Slow migration of mobilised fines during flow in reservoir rocks: laboratory study. J. Pet. Sci. Eng. **122**, 534–541 (2014)
Payatakes, A.C., Tien, C., Turian, R.M.: A new model for granular porous media. I. Model formulation. AIChE J. **19**(1), 58–76 (1973)
Polyanin, A.D. (ed.): The World of Mathematical Equations. http://eqworld.ipmnet.ru/en/auxiliary/aux-integrals.htm. Accessed on 19 Aug 2016 (2016)
Polyanin, A.D., Manzhirov, A.V.: Handbook of Mathematics for Engineers and Scientists. CRC Press, New York (2006)
Polyanin, A.D., Zaitsev, V.F.: Handbook of Nonlinear Partial Differential Equations. Chapman and Hall/CRC, New York (2011)
Schembre, J.M., Kovscek, A.R.: Mechanism of formation damage at elevated temperature. J. Energy Res. Technol. **127**(3), 171–180 (2005)
Schembre, J.M., Tang, G.Q., Kovscek, A.R.: Wettability alteration and oil recovery by water imbibition at elevated temperatures. J. Pet. Sci. Eng. **52**(1), 131–148 (2006)
Sefrioui, N., Ahmadi, A., Omari, A., Bertin, H.: Numerical simulation of retention and release of colloids in porous media at the pore scale. Colloids Surf. A Physicochem. Eng. Asp. **427**, 33–40 (2013)
Sen, T.K., Mahajan, S.P., Khilar, K.C.: Colloid-associated contaminant transport in porous media: 1. Experimental studies. AIChE J. **48**(10), 2366–2374 (2002)
Shapiro, A.A.: Elliptic equation for random walks. Application to transport in microporous media. Phys. A **375**(1), 81–96 (2007)
Shapiro, A.A., Wesselingh, J.A.: Gas transport in tight porous media: gas kinetic approach. Chem. Eng. J. **142**(1), 14–22 (2008)
Sharma, M.M., Yortsos, Y.C.: Fines migration in porous media. AIChE J. **33**(10), 1654–1662 (1987)
Tufenkji, N., Elimelech, M.: Correlation equation for predicting single-collector efficiency in physicochemical filtration in saturated porous media. J. Environ. Sci. Technol. **38**, 529–536 (2004)
Tufenkji, N.: Colloid and microbe migration in granular environments: a discussion of modelling methods. In: Frimmel, F.H., von der Kammer, F., Flemming, H.-C. (eds.) Colloidal Transport in Porous Media, pp. 119–142. Springer, Berlin (2007)

Yang, Y., Siqueira, F., Vaz, A., You, Z., Bedrikovetsky, P.: Slow migration of detached fine particles over rock surface in porous media. J. Nat. Gas Sci. Eng. **34**, 1159–1173 (2016)
You, Z., Bedrikovetsky, P., Badalyan, A., Hand, M.: Particle mobilization in porous media: temperature effects on competing electrostatic and drag forces. Geophys. Res. Lett. **42**(8), 2852–2860 (2015)
You, Z., Yang, Y., Badalyan, A., Bedrikovetsky, P., Hand, M.: Mathematical modelling of fines migration in geothermal reservoirs. Geothermics **59**, 123–133 (2016)
Yuan, B., Moghanloo, R.G., Zheng, D.: Analytical evaluation of nanoparticle application to mitigate fines migration in porous media. J. Soc. Pet. Eng. SPEJ **21**(3), 1–16 (2016)
Yuan, H., Shapiro, A.A.: Modeling non-Fickian transport and hyperexponential deposition for deep bed filtration. Chem. Eng. J. **162**(3), 974–988 (2010)
Yuan, H., Shapiro, A.A.: A mathematical model for non-monotonic deposition profiles in deep bed filtration systems. Chem. Eng. J. **166**(1), 105–115 (2011a)
Yuan, H., Shapiro, A.A.: Induced migration of fines during waterflooding in communicating layer-cake reservoirs. J. Pet. Sci. Eng. **78**(3–4), 618–626 (2011b)
Yuan, H., Shapiro, A.A., You, Z., Badalyan, A.: Estimating filtration coefficients for straining from percolation and random walk theories. Chem. Eng. J. **210**, 63–73 (2012)
Zeinijahromi, A., Lemon, P., Bedrikovetsky, P.: Effects of induced migration of fines on water cut during waterflooding. J. Pet. Sci. Eng. **78**, 609–617 (2011)
Zeinijahromi, A., Al-Jassasi, H., Begg, S., Bedrikovetski, P.: Improving sweep efficiency of edge-water drive reservoirs using induced formation damage. J. Pet. Sci. Eng. **130**, 123–129 (2015)
Zeinijahromi, A., Farajzadeh, R., Bruining, J., Bedrikovetsky, P.: Effect of fines migration on oil–water relative permeability during two-phase flow in porous media. Fuel **176**, 222–236 (2016)